Soft Matter

Dynamic Article Links

Cite this: *Soft Matter*, 2011, **7**, 10720

www.rsc.org/softmatter

PAPER

From diffusive motion to local aggregation: Effect of surface contamination in dipolophoresis†

Jae Sung Park and David Saintillan*

Received 22nd June 2011, Accepted 24th August 2011
DOI: 10.1039/c1sm06172k

We investigate the effects of surface contamination, modeled as a thin dielectric coating, on the dynamics in suspensions of ideally polarizable spheres in an applied electric field using large-scale direct particle simulations. In the case of clean particles (no contamination), the suspensions are known to undergo dipolophoresis, or a combination of dielectrophoresis, which tends to cause particle chaining and aggregation, and induced-charge electrophoresis, which dominates the dynamics and drives transient pairings, chaotic motions, and hydrodynamic diffusion at long times. As surface contamination becomes significant, induced-charge electrophoresis is gradually suppressed, which results in the simulations in a transition from diffusive dynamics to local aggregation and chaining as a result of dielectrophoresis. This effect has a strong impact on the suspension microstructure, as well as on particle velocities, which are strongly reduced for contaminated particles. This transition is also visible in the particle mean-square displacements, which become sub-diffusive in the case of strong contamination. We explain this sub-diffusive regime as a consequence of the slow dynamics of the particles trapped inside clusters and chains, which result in non-integrable local waiting time distributions.

1. Introduction

The ability to control and direct the motion of colloids and nanoparticles suspended in a fluid is critical to many applications in micro- and nanofluidics,[1–6] as well as in materials processing and manufacturing.[7–10] As a result, there has been much interest over the last few years in modeling and understanding the dynamics of particles in electric fields, as these offer a simple and low-cost means of directing particle motions. Specifically, linear electrophoresis (EP), which results from the interaction of the native Debye layer surrounding a charged particle in a viscous electrolyte with an externally applied electric field, drives a net linear motion in the direction of the local field, with a velocity that scales linearly with field strength.[11–13] Under the classic assumptions of thin Debye layer, weak applied field, zero polarizability and surface conduction, EP does not result in relative motions between particles, which instead all migrate at the same velocity, unaffected by interactions.[14–17] Interactions and relative motions, however, often arise when some of these assumptions are relaxed, notably in moderate fields and with polarizable particles.[18]

Department of Mechanical Science and Engineering, University of Illinois at Urbana-Champaign, Urbana, IL 61801, USA. E-mail: dstn@illinois.edu

† Electronic supplementary information (ESI) available: Movie showing the dynamics in suspensions undergoing dipolophoresis at different values of the correction factor Λ, corresponding to different levels of surface contamination. See DOI: 10.1039/c1sm06172k

First, any particle placed in an electric field disturbs the field around it, resulting in a non-uniform Maxwell stress tensor in the fluid, which can yield a non-zero force and torque on surrounding particles.[19,20] These dielectrophoretic (DEP) forces and torques scale quadratically with the field magnitude, and can lead to relative motions in particle suspensions under moderate field strengths.[18,21,22] Second, if the particle is ideally polarizable (*e.g.* conducting), it also develops a non-uniform surface charge distribution in addition to its native charge, which causes the formation of a non-uniform electrical double layer around its surface. The external field then drives an additional flow near the particle surface, which results from the interaction of the induced double layer with the applied field and also scales quadratically with field strength.[23–25] By symmetry, this induced-charge electrophoresis (ICEP) does not result in a net motion in the case of a single isolated spherical particle, but relative motions may arise when several particles are present in a suspension.[18,21,26,27]

The motions resulting from DEP and ICEP have been analyzed in the past.[18,21,22] Dielectrophoretic interactions, in the low-frequency and thin-Debye-layer case, result in the formation of particle chains in the direction of the applied field,[20,28–30] which then often merge and rearrange to form complex structures including particle sheets, labyrinthine and cellular patterns, *etc.*[22,31,32] In these suspensions, particle configurations evolve slowly toward a frozen state where particles are trapped in chains or larger structures and only undergo weak motions. On the other hand, induced-charge electrophoresis results in transient particle pairings, by which two nearby particles are attracted in

the field direction, pair up, and separate in a transverse direction.[18,21,26,27] These pairings have been shown to lead to diffusive particle motions at long times, resulting in constant mixing and reorganization of particle configurations.[21,26] When both DEP and ICEP occur, a situation known as dipolophoresis (DIP),[33,34] ICEP has been found to dominate DEP and diffusive motions are predicted.[21]

While the theory of induced-charge electrokinetic flows is well established,[23–25,35,36] quantitative comparisons with experimental measurements have often yielded mixed results.[27,35,37–42] Detailed measurements of induced-charge flows around fixed posts or electrodes have been described in the literature, and typically show velocities that match theoretical predictions qualitatively but are weaker than expected in magnitude.[39] To model this discrepancy, a fitting parameter or "correction factor" Λ is commonly used and is defined as the factor by which the theoretically predicted induced zeta potential (or surface slip velocity) has to be multiplied to match the experimental data.[35,37,38,41,42] Values of Λ can vary wildly and have ranged from 0.0018 to 0.85 in experiments.[35]

While a comprehensive theory explaining this discrepancy is still lacking, evidence points at surface contamination as a possible factor leading to this reduction in velocity.[41] As a model for surface contamination, Pascall and Squires[41] studied the induced-charge flow near a metal electrode coated with a thin dielectric layer of SiO_2, with permittivity ε_s and thickness λ_s, as illustrated in Fig. 1(a) in the case of a spherical particle. This coating has the effect of introducing an additional capacitance $C_s = \varepsilon_s/\lambda_s$ in series with the Debye layer capacitance $C_D = \varepsilon/\lambda_D$, where ε is the permittivity of the electrolyte and λ_D is the Debye length [Fig. 1(b)]. The resulting induced zeta potential is then expressed as

$$\zeta = \frac{\Delta V}{1+\delta}, \tag{1}$$

where ΔV is the total potential drop and δ is the ratio of the Debye layer capacitance to the dielectric layer capacitance, $\delta = C_D/C_s$. Within this model, the correction factor is naturally obtained as $\Lambda = (1+\delta)^{-1}$. This model is appropriate to capture the effects of a solvation (Stern) layer on the electrode or particle surface. Additional effects may also modify the value of Λ, including the dissociation of protons from the dielectric coating into the Debye layer *via* the chemical reaction $SiOH \leftrightarrow SiO^- + H^+$, which introduces an effective buffer capacitance, C_{buff}, in parallel with the Debye layer capacitance [Fig. 1(c)], and modifies the zeta potential as

$$\zeta = \frac{\Delta V}{1+\delta+\beta}, \tag{2}$$

where $\beta = C_{buff}/C_s$. This results in a correction factor given by $\Lambda = (1+\delta+\beta)^{-1}$. These models have been tested against experiments with SiO_2 coatings,[41] as well as self-assembled monolayers of alkanethiol chains,[42] and good agreement has been shown with theory at low frequencies.

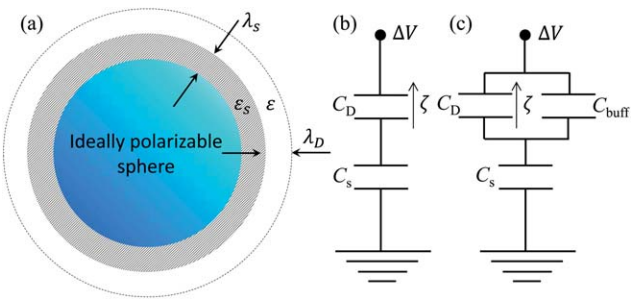

Fig. 1 (a) Model for surface contamination: an ideally polarizable sphere is coated with a thin dielectric layer (not to scale). (b) Circuit model for the situation of (a). (c) Circuit model for the situation of (a) with additional effective buffer capacitance to model dissociation of protons from the dielectric layer.

In a suspension of particles undergoing dipolophoresis in an electrolyte, we expect surface contamination to affect the value of the induced zeta potential leading to induced-charge electrophoresis by a factor of Λ, while dielectrophoretic interactions should be unaffected.[18] The precise effects of such contamination on the suspension dynamics have not been considered to date, and are the subject of the present study. For weak surface contamination ($\Lambda \approx 1$), ICEP is still expected to dominate DEP and lead to diffusive particle motions, whereas stronger contamination ($\Lambda \ll 1$) should nearly suppress ICEP and the formation of chains can be expected as a result of DEP. The dynamics for intermediate values of Λ have not been modeled yet and, as we show below, are characterized by a gradual transition from diffusive motions to local aggregation, chaining, and pattern formation as Λ is decreased. To study this transition, we present a simulation method in section 2 based on our previous model[21] for a periodic suspension of ideally polarizable particles undergoing DIP, in which we introduce the correction factor Λ as a prefactor modulating the magnitude of ICEP with respect to DEP. Results are presented in section 3, where we analyze the effect of Λ on the microstructure, velocity fluctuations, and hydrodynamic diffusion inside the suspensions. We summarize our findings in section 4.

2. Simulation method

We consider a collection of M identical neutrally buoyant polarizable spheres of radius a, suspended in a viscous electrolyte with permittivity ε and viscosity η. A cubic periodic domain of linear dimension L is used to simulate an infinite suspension, and a uniform electric field $\mathbf{E}_0$ is applied in the z-direction: $\mathbf{E}_0 = E_0\hat{\mathbf{z}}$. The particles are assumed to carry no net charge, in which case linear electrophoresis does not occur; it could easily be accounted for by simply adding the constant electrophoretic velocity $(\varepsilon\zeta/\eta)\,\mathbf{E}_0$ to the velocity of each sphere.

We adopt the simulation method developed in our previous work,[21] which was used to simulate the motion of ideally polarizable spheres under DIP, and is based on the calculation of DEP and ICEP interactions by Saintillan.[18] The formulation is valid in the limit of thin Debye layers and for weak constant electric fields, and neglects surface conduction (zero Dukhin number). The reader is referred to these two previous papers[18,21] for a detailed description of the method and algorithm, which are only outlined here. To model surface contamination, we use the correction factor, Λ, introduced above, which modifies the surface slip velocity induced by the electric field:

$$\mathbf{u}_s(\mathbf{x}) = \Lambda \frac{\varepsilon \zeta_i(\mathbf{x}) \mathbf{E}(\mathbf{x})}{\eta}, \tag{3}$$

which drives ICEP fluid motion and particle interactions. As a result, the translational velocity $\mathbf{U}_\alpha$ of particle α located at $\mathbf{x}_\alpha$, which we had calculated in our previous work[21] for clean particles ($\Lambda = 1$), becomes:

$$\mathbf{U}_\alpha = \frac{\varepsilon a E_0^2}{\eta} \sum_{\beta=1}^{M} [\mathbf{M}^{dep}(\mathbf{R}_{\alpha\beta}/\alpha) + \Lambda \mathbf{M}^{icep}(\mathbf{R}_{\alpha\beta}/a)] : \hat{\mathbf{z}}\hat{\mathbf{z}} \tag{4}$$

where $\mathbf{M}^{dep}$ and $\mathbf{M}^{icep}$ are third-order dimensionless tensors accounting for both electric and hydrodynamic interactions of particles α and β under DEP and ICEP, respectively, and $\mathbf{R}_{\alpha\beta}$ denotes the separation vector between the two spheres: $\mathbf{R}_{\alpha\beta} = \mathbf{x}_\beta - \mathbf{x}_\alpha$. The only difference between eqn (4) and that of our previous work[21] is the prefactor Λ, which controls the relative magnitude of DEP and ICEP interactions as a result of contamination. Denoting by $\lambda = 2a/|\mathbf{R}|$ the dimensionless inverse separation distance, Saintillan[18] showed that, based on symmetries, these two tensors are entirely determined by three scalar functions of λ. For far-field interactions ($\lambda \ll 1$), asymptotic expressions for these two tensors have been obtained and can be expressed to order $O(\lambda^4)$ in terms of fundamental solutions of the Stokes equations:

$$\mathbf{M}_{FF}^{dep}(\mathbf{R}/a) = \frac{1}{12}\mathbf{T}(\mathbf{R}/a) + O(\lambda^5), \tag{5}$$

$$\mathbf{M}_{FF}^{icep}(\mathbf{R}/a) = -\frac{9}{8}\mathbf{S}(\mathbf{R}/a) - \frac{11}{24}\mathbf{T}(\mathbf{R}/a) + O(\lambda^5), \tag{6}$$

where $\mathbf{S}$ and $\mathbf{T} = \nabla^2\mathbf{S}$ denote the Green's functions for a Stokes dipole and for a potential quadrupole, respectively, and are given in index notation as[43]

$$S_{ijk}(\mathbf{R}) = -\frac{1}{R^3}(\delta_{ij}R_k - \delta_{ik}R_j - \delta_{jk}R_i) - 3\frac{R_iR_jR_k}{R^5}, \tag{7}$$

$$T_{ijk}(\mathbf{R}) = -\frac{6}{R^5}(\delta_{ij}R_k + \delta_{ik}R_j + \delta_{jk}R_i) + 30\frac{R_iR_jR_k}{R^7}. \tag{8}$$

From the above interaction tensors, it can be seen that ICEP interactions decay slowly in the far-field as $O(\lambda^2)$, as opposed to DEP interactions that decay more rapidly as $O(\lambda^4)$; this results, in the absence of surface contamination, in the dominance of ICEP as demonstrated in our previous study.[21]

In order to use periodic boundary conditions, the periodic analogs of eqn (5)–(6) are used, in conjunction with an efficient smooth particle-mesh Ewald algorithm[44] to accelerate the evaluation of the sums in eqn (4) to $O(M \log M)$ operations. As the far-field tensors of eqn (5)–(6) are only accurate at large separation distances (typically when $|\mathbf{R}_{\alpha\beta}| > 4a$), near-field corrections are applied at shorter distances using the method of twin multipole expansions,[18] which provides very accurate solutions down to separation distances on the order of $|\mathbf{R}_{\alpha\beta}| \approx 2.05a$. In addition, a contact algorithm is also used to prevent particle overlaps, which would otherwise occur because of the use of finite time steps; this algorithm was shown previously to prevent all overlaps within roundoff errors without introducing any unphysical long-range interactions.[21]

In the remainder of the paper, we make all variables dimensionless using the following characteristic length, velocity and time scales:

$$l_c = a, \quad u_c = \frac{\varepsilon a E_0^2}{\eta}, \quad t_c = \frac{\eta}{\varepsilon E_0^2}. \tag{9}$$

Unless otherwise noted, all the simulations described were performed for a suspension of $M = 2000$ spheres in a periodic cubic box of linear dimension $L = 55$, corresponding to a volume fraction of $\phi \approx 5\%$.

3. Results and discussion

3.1 Suspension microstructure

Typical particle distributions in suspensions of 2000 spheres are shown in Fig. 2 for different values of the correction factor Λ (also see accompanying movie in the Supplementary Materials†). In Fig. 2, the top panel shows three-dimensional views of the entire suspensions, whereas the bottom panel shows vertical slices of thickness 5. The case of ideally polarizable spheres with no surface contamination ($\Lambda = 1$), which was analyzed in detail in our previous work,[21] is characterized by frequent transient particle pairings, by which pairs of particles are attracted in the field direction, pair up briefly, and are repelled and separate in a transverse direction. These pairings also result in a weakly non-homogeneous distribution of particles, with local clusters surrounded by clarified regions [Fig. 2(a) and (d)]. As the effective polarizability of the particles is decreased as a result of surface contamination, these transient pairings gradually give way to the formation of larger and denser localized clusters, surrounded by large particle-free regions, as seen in Fig. 2(b) and (e). These clusters, at moderate values of Λ, are still transient, and keep forming and breaking up in time with no fixed membership. As surface contamination becomes yet more significant, induced-charge electrophoresis becomes nearly negligible, and the dynamics become dominated by DEP interactions, which cause the particles to form long chains in the direction of the electric field [Fig. 2(c) and (f)]. These chains, which span the entire height of the simulation box, slowly rearrange and sometimes merge, as

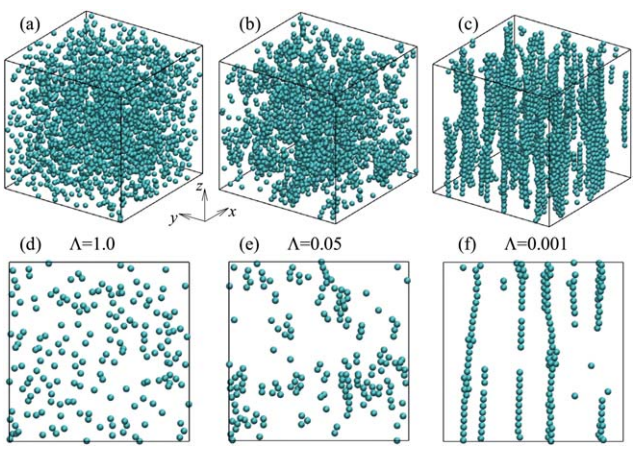

Fig. 2 Steady-state particle distributions in suspensions of $M = 2000$ spheres in a periodic cubic box of dimension $L = 55$ (volume fraction $\phi \approx 5\%$), for different correction factors: (a)–(d) $\Lambda = 1.0$, (b)–(e) $\Lambda = 0.05$, (c)–(f) $\Lambda = 0.001$. Top row: three-dimensional view of the full suspensions; bottom row: vertical slices of thickness 5. Also see accompanying movie in the Supplementary Materials.†

is known to be the case in suspensions undergoing dipolar interactions.[29–32,45–48] These dynamics, in particular, were investigated more precisely in a previous study,[22] where we found that in sufficiently dense confined suspensions (volume fraction $\phi \approx 20\%$ and higher) particles end up forming cellular patterns of particle-rich walls enclosing particle-free voids, in qualitative agreement with previous experiments.[49,50]

The transition from transient unstable pairings to stable pairings and chain formation as surface contamination increases (*i.e.* as Λ decreases) is easily understood from the calculation of pair interactions of Saintillan.[18] Indeed, while both DEP and ICEP interactions are attractive in the field direction but repulsive in the transverse directions, the paired-up configuration (two touching spheres aligned with the field direction) can be shown to be unstable under ICEP but stable under DEP.[18,21] As the relative magnitude of DEP and ICEP is varied as a result of contamination (*via* the correction factor), we therefore expect the nature of the dynamics to change qualitatively. This is described more precisely in Fig. 3, showing the critical value Λ_c of the correction factor below which DEP starts dominating ICEP, as a function of the distance between the two spheres. More precisely, Λ_c is defined as the value of Λ for which the relative velocity between two interacting spheres at a given separation distance has zero component in the direction normal to the line of centers (see inset of Fig. 3). In particular, for two touching spheres ($|\mathbf{R}| = 2a$), we find that the paired-up configuration will be stable if $\Lambda \leq \Lambda_c \approx 0.03$: below this value of Λ, we expect chaining to take place in the suspensions, whereas chaining should not occur above this value. The critical value of $\Lambda_c \approx 0.03$ for the transition from diffusive dynamics to chaining is consistent with the observations of Fig. 2, as well as with the rest of the data as we show below.

To further characterize the particle distributions observed in Fig. 2, we calculate particle occupancy statistics, which provide information on the number density fluctuations at arbitrary length scales. Specifically, Fig. 4(a) shows the distribution $P(N)$

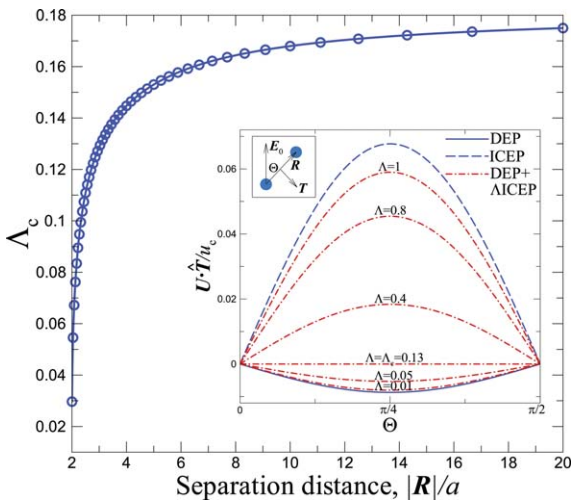

Fig. 3 Critical value Λ_c of the correction factor below which DEP interactions start dominating ICEP interactions, as a function of the distance between two spheres. Inset: Relative tangential velocity between two spheres as a function of the angle Θ between the direction of the spheres and the direction of the field, for various values of Λ, for two spheres at a distance of $2.5a$.

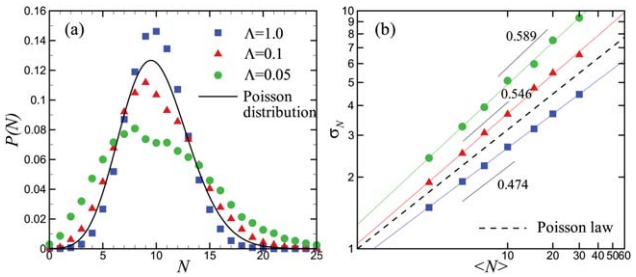

Fig. 4 (a) Particle occupancy distributions for $\langle N \rangle = 10$ at different Λ. (b) Standard deviations of the number of particles as a function of $\langle N \rangle$ for various Λ.

of the number N of particles found in a cubic interrogation cell of a size such that it should contain $\langle N \rangle = 10$ particles on average. This distribution, in the case of a fully random suspension obeying Poisson statistics, should follow the Poisson law:

$$P(N) = \frac{\langle N \rangle^N e^{-\langle N \rangle}}{N!}, \tag{10}$$

and departures from this law provide information on the structure of the suspension on the scale of the interrogation cell. In the absence of surface contamination ($\Lambda = 1$), we find that the distribution $P(N)$ is slightly narrower than the Poisson distribution, which indicates smaller number density fluctuations than in a random suspension; this observation is likely an effect of the moderate volume fraction used in the simulations, whereas the Poisson distribution does not account for excluded volume and should therefore only be observed in the limit of infinite dilution. However, as Λ decreases, the distribution $P(N)$ is found to become flatter and broader than the Poisson distribution, which indicates the presence of clusters and depleted regions in the suspension, in agreement with the observations on Fig. 2. To quantify the influence of scale, *i.e.* of $\langle N \rangle$, on these distributions, we also plot in Fig. 4(b) the standard deviation σ_N of the distributions *vs.* the expected value $\langle N \rangle$, for three values of Λ. In the case of a Poisson distribution, a power law with exponent 1/2 is theoretically predicted: $\sigma_N = \langle N \rangle^{1/2}$. Here, we find that the standard deviations are also well-fitted by a power law, $\sigma_N = \langle N \rangle^n$, with an exponent n that deviates slightly from 1/2 and depends on the importance of surface contamination. In agreement with Fig. 4(a), we observe that $n \lesssim 1/2$ for $\Lambda = 1$, whereas it increases beyond 1/2 as Λ decreases, indicating an increase in number density fluctuations at all scales as a result of the dominant DEP interactions.

3.2 Pairing dynamics

As mentioned in section 3.1, the distinct microstructures that develop in the suspensions depending on the value of the correction factor Λ can be explained in terms of pair interactions, which cause transient pairings when $\Lambda_c < \Lambda \leq 1$ as a result of ICEP, and the formation of clusters and chains when $\Lambda \leq \Lambda_c$ as a result of DEP. Here, we further analyze pair dynamics in our simulations, and show in Fig. 5 the time evolution of the separation distance between a test sphere in the suspension and its nearest neighbor. In the absence of contamination [$\Lambda = 1$, Fig. 5 (a)], the minimum distance constantly fluctuates between a value

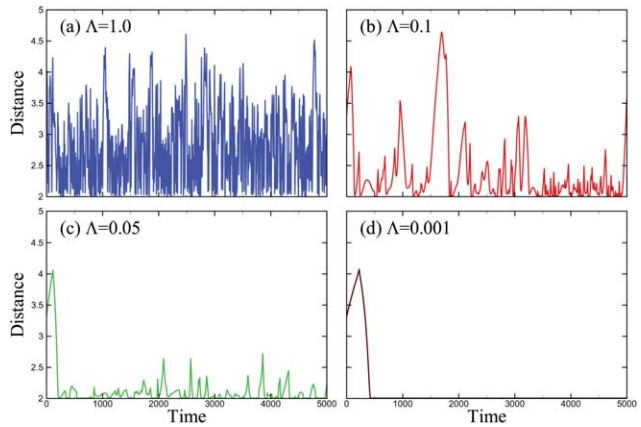

Fig. 5 Separation distance from a test sphere to its nearest neighbor at different correction factors Λ.

of two particle radii, corresponding to near contact between the test sphere and its closest neighbor, to a larger value on the order of the mean interparticle distance $a\phi^{-1/3}$. These oscillations, which are consistent with our previous work,[21] again demonstrate the transient character of particle pairings under ICEP, by which a particle keeps pairing with its neighbors without forming lasting clusters. As surface contamination becomes significant, the distance to the nearest neighbor is found to decrease, and fluctuates near a value that is close to two particle radii: this indicates that pairings now become long-lasting, as expected from DEP interactions, which become more significant. This is very clear for low values of the correction factor [especially $\Lambda = 0.001$, Fig. 5(d)], when the test particle is seen to pair up quickly with another particle and then remain attached to it (or possibly another particle) for the remainder of the simulation, as demonstrated by a distance of exactly $2a$ to the nearest particle.

Another way of quantifying these pairings is to consider the pair distribution function in the suspension, $p(r, z)$, in cylindrical coordinates (where $r^2 = x^2 + y^2$). This function describes the probability of finding a particle at position (r, z) knowing that a particle is located at the origin. This function is shown in Fig. 6 for two different values of the correction factor Λ. In both cases, a region of excluded volume is observed inside the circle of radius $2a$, and the distribution function exhibits a sharp peak near the pole of the particle, corresponding to a high probability of finding two particles paired up and aligned in the field direction. On the other hand, a low-probability depletion region is

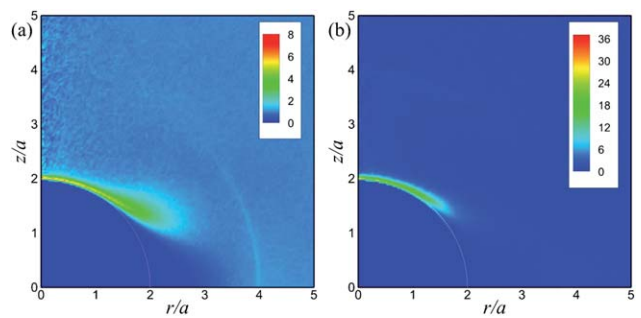

Fig. 6 Steady-state pair distribution functions for various correction factors: (a) $\Lambda = 1.0$ and (b) $\Lambda = 0.1$.

observed near the equator, as two particles that are side by side are repelled under both DEP and ICEP. Similar findings had been made in previous studies on DIP of sphere suspensions without surface contamination,[21] and on ICEP in suspensions of rod-like particles.[26,27] The peak near the pole in Fig. 6 is observed for both $\Lambda = 1$ and $\Lambda = 0.1$, as both DEP and ICEP result in pairings, but the peak is found to be stronger and more concentrated at the pole for lower values of Λ, as the pairings are longer-lasting owing to stronger DEP interactions.

Pair distributions in the case of strong contamination ($\Lambda = 0.001$) are also shown in Fig. 7, where the logarithm of $p(r, z)$ is shown at different times (where $t = 0$ corresponds to a random distribution of particles). At this low value of Λ, we know from Fig. 2 that particles aggregate into chains in the field direction. This is reflected in the distribution function, which develops a clear succession of peaks along the z-axis at $z = 2a$, $4a$, $6a$, and $8a$. Circles emanating from these peaks are also observed, as the chains are not completely straight in the z-direction but often curve, see Fig. 2(f). In addition to these primary peaks, other weaker peaks are also observed at $z = 2\sqrt{3}a$, $4\sqrt{2}a$, *etc.* These cannot be explained by the formation of straight chains, but instead result from the coalescence of nearby chain segments into hexagonal structures (typically sheets), as previously observed in other simulations.[22]

3.3 Hydrodynamic dispersion and velocity fluctuations

Previous investigations have shown that dipolophoresis, in the absence of surface contamination, results in an effective diffusive motion of the suspended particles at long times, as a result of the frequent pairings driven by hydrodynamic interactions.[21,26] This hydrodynamic diffusion is a consequence of ICEP, which constantly causes the particle configurations to rearrange without the formation of any long-lasting structures or clusters. If surface contamination becomes significant, we have shown

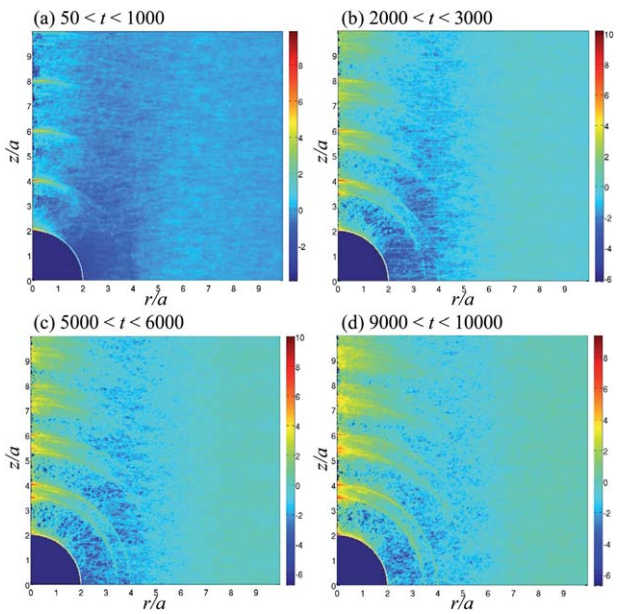

Fig. 7 Time evolution of the pair distribution function for a correction factor of $\Lambda = 0.001$.

that DEP interactions become more important and eventually dominate, in which case pairings are no longer transient and instead result in the formation of chains. In this case, we no longer expect the particle motions to be diffusive, as particles get effectively trapped in chains or larger structures, which hinders their ability to diffuse in space.

To quantify this effect more precisely, we plot mean-square particle displacements *vs.* time in Fig. 8 for different values of the correction factor Λ. All plots first exhibit a quadratic growth at short times (as demonstrated by a slope of 2 in a log–log plot), corresponding to a ballistic regime. This ballistic regime is then followed by a second regime characterized by a slower growth of the mean-square displacements. For weak surface contamination [$\Lambda = 1.0$ and 0.1, Fig.8(a)–(b)], this second regime is diffusive as demonstrated by a slope of 1 in a log–log plot: this is consistent with previous investigations,[21,26] and is a result of the unstable pairings that occur in the suspensions and cause particles to constantly travel in a chaotic fashion. Interestingly, when surface contamination becomes more significant, the ballistic regime gives way to a sub-diffusive regime, with a growth of mean-square displacements as t^{α} with an exponent $\alpha < 1$ that differs between the field direction (z-direction) and transverse directions (x- and y-directions). This is illustrated more precisely, in Fig. 9 (a), showing the dependence of the long-time exponent α *versus* the correction factor Λ, in both the x- and z-directions. While both exponents are 1 for $\Lambda \gtrsim 0.05$, they are observed to decay to sub-diffusive values at lower values of Λ. The dependence on volume fraction is also shown in Fig. 9(b) in the case of strong contamination ($\Lambda = 0.001$), where it is seen that the exponent α increases with ϕ, as a result of the stronger fluctuations arising from interactions in more concentrated suspensions. Note in Fig. 9 that the exponents for the x-direction seem to be less affected by the transition than they are for the z-direction: this can be explained by the alignment of the chains with the field direction, which strongly constrains particle motions in the z-direction while still allowing motions in the transverse x- and y-directions.

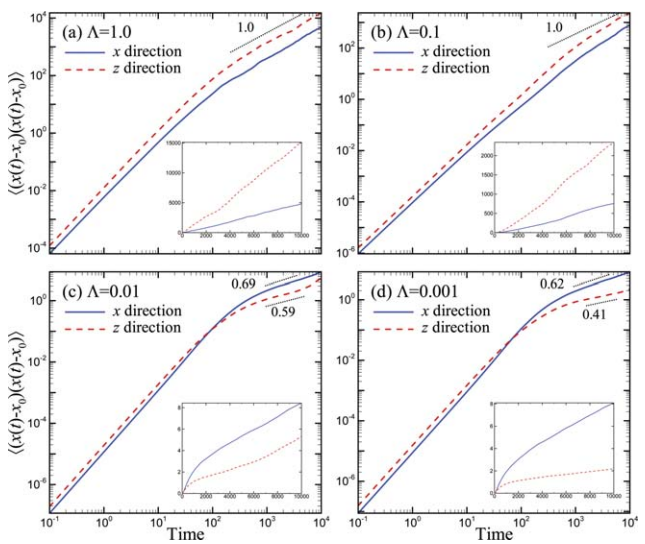

Fig. 8 Mean-square particle displacements in the x- and z-directions for various values of Λ, in log–log scale. Insets: linear plots.

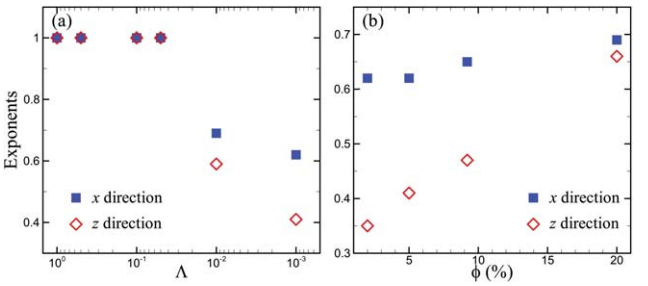

Fig. 9 (a) Exponents of mean-square displacement curves at long times ($\phi = 5\%$). Note the inverted scale for Λ. (b) Exponents of mean-square displacement curves at long times for $\Lambda = 0.001$ *versus* volume fraction ϕ.

The transition from diffusive motion as a result of pairings to sub-diffusion as a result of aggregation and chaining also has a strong impact on the magnitude of particle velocities, which are strongly reduced when chaining takes place. This is illustrated in Fig. 10, showing the standard deviation of the x and z components of the particle velocities as functions of the correction factor (note that the mean velocity of the suspension is exactly zero in the absence of linear electrophoresis). We find that as Λ decreases (*i.e.* as contamination increases) particle velocities become very weak in both directions. Interestingly, while velocities in the field direction (z-direction) are the strongest when $\Lambda \approx 1$ (in agreement with our previous study[21]), horizontal velocities become dominant when chaining occurs at lower values of Λ, owing once again to the constraint on vertical motions when particles are trapped inside chains.

To elucidate the transition from diffusion to sub-diffusion with decreasing Λ, we picture the dynamics of a particle in the suspension as a succession of random displacements separated by waiting periods during which the particle stops (or nearly stops) moving in space (typically during a pairing event, or because it gets trapped in a cluster or chain). Defining the waiting times τ_x and τ_z as the times during which either $|U_x|$ or $|U_z|$ remains less than 25% of the velocity standard deviation in that direction, we plot in Fig. 11 the distributions $\varphi(\tau_x)$ and $\varphi(\tau_z)$ of waiting times in the field and transverse directions for different values of Λ. When surface contamination is weak ($\Lambda = 1.0$ and 0.1), the distributions decay faster than algebraically. This changes qualitatively for stronger contamination ($\Lambda = 0.01$ and 0.001), where the distributions start exhibiting a power-law decay of the form $\varphi(\tau)$

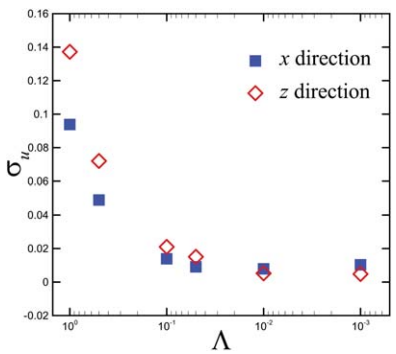

Fig. 10 Standard deviation of particle velocities in the x- and z-directions as functions of Λ.

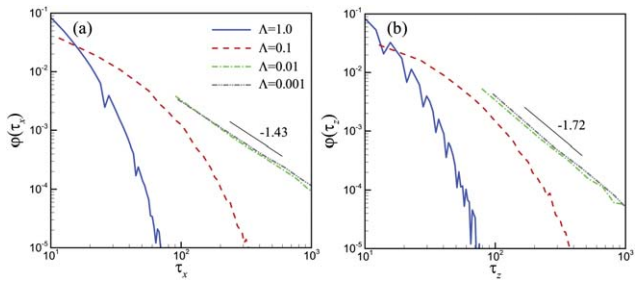

Fig. 11 Distributions $\varphi(\tau_x)$ and $\varphi(\tau_z)$ of waiting times in the (a) x- and (b) z-directions, for different values of Λ. A waiting time τ_x or τ_z is defined a period of time during which $|U_x|$ or $|U_z|$ remains less than 25% of the velocity standard deviation in that direction.

$\sim \tau^{-(1+\alpha)}$, with $\alpha < 1$. Such non-integrable distributions of waiting times have been shown previously to result in sub-diffusion,[51,52] with mean-square displacements growing as $\sim t^{\alpha}$. The value of the coefficient α, extracted from the distributions of Fig. 11, ranges from ≈ 0.4 to ≈ 0.7. While these estimates do not perfectly match the growth exponents found in Fig. 9 for the mean-square displacements, they are fairly close in magnitude. This strongly suggests that the sub-diffusive regime discussed above is indeed a consequence of the long waiting times (with non-integrable distributions) that arise once particles form larger structures and become trapped inside clusters and chains.

4. Summary

We have used numerical simulations to study the effects of surface contamination on the dynamics of suspensions of polarizable spheres under dipolophoresis, or combination of dielectrophoresis and induced-charge electrophoresis. Following previous investigations in this area, we modeled surface contamination by means of a correction factor $\Lambda \leq 1$ that multiplies the induced-charge slip velocity driving ICEP, and therefore modulates the relative importance of DEP and ICEP interactions in dipolophoresis. This correction factor, which is generally measured in experiments, can be rationalized from simple models of surface contamination based on thin dielectric coatings or ion surface adsorption.

The main finding from our simulations is the existence of a transition as surface contamination becomes significant (*i.e.* as Λ decreases) from transient local pairing dynamics (owing to the dominant ICEP interactions in the case of clean particles) to local aggregation, cluster formation and chaining (owing to the dominant DEP interactions in the case of contaminated particles, for which ICEP is nearly suppressed). This transition can be explained based on a simple analysis of pair interactions, which shows that particle chaining is stable under DEP but unstable under ICEP. In addition to qualitatively modifying the microstructure and morphology of the suspension, this transition has a significant impact on particle velocities, which are strongly reduced, in particular in the field direction. It also modifies qualitatively the statistical nature of particle motions at long times, which is diffusive in the case of clean particles, but sub-diffusive in the case of contaminated particles. Further, this sub-diffusive regime was shown to be linked to the slow decay of the local waiting time distributions, which become non-integrable after the transition to chaining owing to the frequent trapping of particles inside larger structures.

Acknowledgments

The authors are grateful to Antonio Ramos (University of Sevilla) and Sascha Hilgenfeldt (University of Illinois) for suggesting to investigate this problem. This work was supported in part by Lawrence Livermore National Laboratory under Subcontract No. DOE-B583843.

References

1 T. M. Squires and S. R. Quake, *Rev. Mod. Phys.*, 2005, **77**, 977–1026.
2 X. Y. Hu, P. H. Bessette, J. R. Qian, C. D. Meinhart, P. S. Daugherty and H. T. Soh, *Proc. Natl. Acad. Sci. U. S. A.*, 2005, **102**, 15757.
3 A. E. Cohen and W. E. Moerner, *Appl. Phys. Lett.*, 2005, **86**, 093109.
4 S. J. Williams, A. Kumar, N. G. Green and S. T. Wereley, *J. Micromech. Microeng.*, 2010, **20**, 015022.
5 L. Shui and S. Pennathur, *Lab Chip*, 2008, **8**, 1010–1014.
6 M. T. Napoli, P. Atzberger and S. Pennathur, *Microfluid. Nanofluid.*, 2011, **10**, 69.
7 S.-R. Yeh, M. Seul and B. I. Shraiman, *Nature*, 1997, **386**, 57.
8 X. G. Xiong, P. Makaram, A. Busnaina, K. Bakhtari, S. Somu, N. McGruer and J. Park, *Appl. Phys. Lett.*, 2006, **89**, 193108.
9 S. J. Williams, A. Kumar and S. T. Wereley, *Lab Chip*, 2008, **89**, 193108.
10 Y. S. Joung and C. R. Buie, *Langmuir*, 2011, **27**, 4156–4156.
11 D. A. Saville, *Annu. Rev. Fluid Mech.*, 1977, **9**, 321–337.
12 J. L. Anderson, *Annu. Rev. Fluid Mech.*, 1989, **21**, 61–99.
13 W. B. Russel, D. A. Saville and W. R. Schowalter, *Colloidal dispersions*, Cambridge University Press, 1989.
14 L. D. Reed and F. A. Morrison, *J. Colloid Interface Sci.*, 1975, **54**, 117–133.
15 S. B. Chen and H. J. Keh, *AIChE J.*, 1988, **34**, 1075–1085.
16 A. Acrivos, D. J. Jeffrey and D. A. Saville, *J. Fluid Mech.*, 1990, **212**, 95–110.
17 N. A. Patankar, *Mech. Res. Commun.*, 2009, **36**, 39–45.
18 D. Saintillan, *Phys. Fluids*, 2008, **20**, 067104.
19 H. A. Pohl, *Dielectrophoresis*, Cambridge University Press, 1978.
20 T. B. Jones, *Electromechanics of Particles*, Cambridge University Press, 1995.
21 J. S. Park and D. Saintillan, *J. Fluid Mech.*, 2010, **662**, 66–90.
22 J. S. Park and D. Saintillan, *Phys. Rev. E: Stat., Nonlinear, Soft Matter Phys.*, 2011, **83**, 041409.
23 M. Z. Bazant and T. N. Squires, *Phys. Rev. Lett.*, 2004, **15**, 203–213.
24 T. M. Squires and M. Z. Bazant, *J. Fluid Mech.*, 2004, **509**, 217–252.
25 T. M. Squires and M. Z. Bazant, *J. Fluid Mech.*, 2006, **560**, 65–101.
26 D. Saintillan, E. Darve and E. S. G. Shaqfeh, *J. Fluid Mech.*, 2006, **563**, 223–259.
27 K. A. Rose, B. Hoffman, D. Saintillan, E. S. G. Shaqfeh and J. G. Santiago, *Phys. Rev. E: Stat., Nonlinear, Soft Matter Phys.*, 2009, **79**, 011402.
28 A. A. Füredi and R. C. Valentine, *Biochim. Biophys. Acta*, 1962, **56**, 33.
29 T. C. Halsey and W. Toor, *Phys. Rev. Lett.*, 1990, **65**, 2820.
30 E. M. Furst and A. P. Gast, *Phys. Rev. E: Stat. Phys., Plasmas, Fluids, Relat. Interdiscip. Top.*, 2000, **62**, 6916.
31 J. E. Martin, R. A. Anderson and C. P. Tigges, *J. Chem. Phys.*, 1998, **108**, 3765.
32 U. Dessanayake, S. Fraden and A. van Blaaderen, *J. Chem. Phys.*, 2000, **112**, 3851.
33 V. N. Shilov and T. S. Simonova, *Colloid J. USSR*, 1981, **43**, 90–96.
34 T. Miloh, *Phys. Fluids*, 2008, **20**, 063303.
35 M. Z. Bazant, M. S. Kilic, B. D. Storey and A. Ajdari, *Adv. Colloid Interface Sci.*, 2009, **152**, 48–88.
36 M. Z. Bazant and T. M. Squires, *Curr. Opin. Colloid Interface Sci.*, 2010, **15**, 203–213.
37 N. G. Green, A. Ramos, A. González, H. Morgan and A. Castellanos, *Phys. Rev. E: Stat. Phys., Plasmas, Fluids, Relat. Interdiscip. Top.*, 2000, **61**, 4011–4018.

38 N. G. Green, A. Ramos, A. González, A. Castellanos and H. Morgan, *Phys. Rev. E: Stat. Phys., Plasmas, Fluids, Relat. Interdiscip. Top.*, 2002, **66**, 026305.
39 J. A. Levitan, S. Devasenathipathy, V. Studer, Y. Ben, T. Thorsen, T. M. Squires and M. Z. Bazant, *Colloids Surf., A*, 2005, **267**, 122–132.
40 S. Gangwal, O. J. Cayre, M. Z. Bazant and O. D. Velev, *Phys. Rev. Lett.*, 2008, **100**, 058302.
41 A. J. Pascall and T. M. Squires, *Phys. Rev. Lett.*, 2010, **104**, 088301.
42 J. Pascall and T. M. Squires, *Lab Chip*, 2010, **10**, 2350–2357.
43 S. Kim and S. P. Karrila, *Microhydrodynamics: Principles and Selected Applications*, Butterworth-Heinemann, 1991.
44 D. Saintillan, E. Darve and E. S. G. Shaqfeh, *Phys. Fluids*, 2005, **17**, 033301.
45 T. C. Halsey and W. Toor, *J. Stat. Phys.*, 1990, **61**, 1257.
46 J. E. Martin, J. Odinek and T. C. Halsey, *Phys. Rev. Lett.*, 1992, **69**, 1524.
47 M. Gross and S. Kiskamp, *Phys. Rev. Lett.*, 1997, **79**, 2566.
48 Khusid and A. Acrivos, *Phys. Rev. E: Stat. Phys., Plasmas, Fluids, Relat. Interdiscip. Top.*, 1999, **60**, 3015.
49 A. Kumar, B. Khusid, Z. Y. Qiu and A. Acrivos, *Phys. Rev. Lett.*, 2005, **95**, 258301.
50 K. Agarwal and A. Yethiraj, *Phys. Rev. Lett.*, 2009, **102**, 198301.
51 J. P. Bouchaud and A. Georges, *Phys. Rep.*, 1990, **127**, 127–293.
52 Q. Xu, L. Feng, R. Sha, N. C. Seeman and P. M. Chaikin, *Phys. Rev. Lett.*, 2011, **106**, 228102.